JOURNAL OF APPLIED PHYSICS **119**, 065103 (2016)

Effect of interlayer on interfacial thermal transport and hot electron cooling in metal-dielectric systems: An electron-phonon coupling perspective

Yan Wang,[1] Zexi Lu,[1] Ajit K. Roy,[2] and Xiulin Ruan[1,a)]
[1]*School of Mechanical Engineering and the Birck Nanotechnology Center, Purdue University, West Lafayette, Indiana 47907, USA*
[2]*Materials and Manufacturing Directorate, Air Force Research Laboratory, Wright Patterson Air Force Base, Dayton, Ohio 45433, USA*

(Received 18 November 2015; accepted 23 January 2016; published online 11 February 2016)

It was reported that an interlayer with intermediate phonon spectra between two dielectric materials could reduce the phononic interfacial thermal resistance. In this work, we show that an appropriate choice of interlayer materials with relatively strong electron-phonon coupling could significantly enhance interfacial thermal transport across metal-dielectric interfaces. Our Boltzmann transport simulations demonstrate that such enhancement is achieved by the elimination of electron-phonon nonequilibrium near the original metal-dielectric interface. Moreover, we reveal that interlayer can substantially accelerate hot electron cooling in thin films with weak electron-phonon coupling, for example, Cu, Ag, and Au, supported on a dielectric substrate. At the same time, lattice heating in the thin film is largely reduced. © *2016 AIP Publishing LLC*. [http://dx.doi.org/10.1063/1.4941347]

I. INTRODUCTION

As the feature size in many current and emerging electronic and photonic devices shrinks to the sub-100 nm regime, interfaces between different components begin to dominate the overall heat transfer characteristics.[1] Controlling interfacial thermal transport has thereby become an inevitable challenge for thermal management of those devices.

In addition to engineering the thermal conductivity of materials for thermal management,[2–8,49] previous studies have also demonstrated various schemes to manipulate thermal transport across solid-solid interfaces, for example, introduction of interface roughness,[9] modification of interfacial bonding,[10–12] hierarchical alignment of multiple interfaces,[13–15] and insertion of an interlayer with intermediate vibrational properties between the two materials.[11,16] The aforementioned schemes primarily focus on engineering phonon transport, while much less attention[17–19] was paid to the electron side. Moreover, it was revealed that electron-phonon interaction plays an important role in thermal transport across metal-dielectric interfaces,[20,21] suggesting the feasibility of controlling interfacial thermal transport by manipulating the electron degree-of-freedom.

The coexistence of electron and phonon channels, however, makes thermal transport occur in a rather complicated manner. In pump-probe experiments,[22] for instance, laser radiation rapidly elevates the electron temperature to thousands of Kelvin in a time scale of tens to hundreds of femtoseconds, while the lattice (phonons) remains cool. Subsequently, the deposition of heat from hot electrons to cold phonons occurs in a time scale of the order of electron-phonon relaxation time (1–10 ps), which renders the electrons and phonons almost in thermal equilibrium with each other yet still at a temperature higher than the substrate. Finally, the gradual heat dissipation across the interface and then into the substrate starts to dominate in a time span of nanoseconds. Obviously, the transient thermal process described above is characterized by the dominance of different thermal transport channels in a sequential manner. In contrast, steady-state thermal transport reflects the summation of all the existing channels. A rigorous understanding of the above thermal transport processes is therefore important for the management of the overall heat transfer characteristics of electronic and photonic devices.

In this work, we strive to understand various heat transfer pathways and evaluate the effect of interlayer on interfacial thermal transport and hot electron cooling dynamics in metal-dielectric systems. In our previous work, we estimated that the interfacial thermal conductance of Au-Si interface could be significantly enhanced by adding a thin interlayer of metal with strong electron-phonon coupling, such as Al, Ni, Ti, and Cr.[18] This is because such an interlayer can readily drag electron and phonon into thermal equilibrium, which reduces the thermal resistance associated with the electron-phonon nonequilibrium near the metal-semiconductor interface.[21] Herein we perform more quantitative predictions, including relevant electron-phonon coupling and phonon transmission processes, to show that applying an appropriate interlayer can be a practical way to enhance thermal transport across metal-dielectric interfaces. Moreover, we also evaluate the effect of interlayer on hot electron cooling dynamics during ultrafast laser heating. We will show that this is of practical importance because of interlayer's two competing effects on a device: on one hand, it reduces lattice heating and thereby extending device lifetime; on the other hand, it accelerates the energy loss of hot electrons, which degrades energy efficiency.

This paper proceeds as follows. In Section II, we describe the two-temperature Boltzmann transport equation (BTE) method to simulate electron-phonon coupled thermal transport. In Section III, we briefly present calculations of

a)Electronic mail: ruan@purdue.edu

the input parameters for the BTE simulations, such as electronic/phononic thermal conductivity and interfacial thermal conductance. In Section IV, we evaluate the effect of Al and Pt interlayers on steady-state interfacial thermal transport and ultrafast hot electron cooling dynamics in Au-Si systems.

II. TWO-TEMPERATURE BOLTZMANN TRANSPORT EQUATION

We combine the BTE method with the two-temperature model (TTM) by including an electron-phonon coupling term in both the phononic and the electronic BTEs

$$\frac{\partial e_e}{\partial t} + \mathbf{v_e} \cdot \nabla e_e = \frac{e_e^0 - e_e}{\tau_e} - G_{ep}(T_e - T_p) + \dot{r}_e, \tag{1a}$$

$$\frac{\partial e_p}{\partial t} + \mathbf{v_p} \cdot \nabla e_p = \frac{e_p^0 - e_p}{\tau_p} + G_{ep}(T_e - T_p) + \dot{r}_p, \tag{1b}$$

where e_e and e_p are the energy density of electrons and phonons,[23,24] respectively, and G_{ep} is the electron-phonon coupling constant. e_e and e_p are related to the electron and phonon temperatures via $e_e = 0.5\gamma_e T_e^2$[25] and $e_p = C_p T_p$ (classical limit), where γ_e is the electron heat capacity constant and C_p is the phonon heat capacity. In addition, $\mathbf{v}$ denotes velocity, τ is relaxation time, and $\dot{r}$ is volumetric heat generation rate.

The lattice Boltzmann method[26] (LBM) is used to solve the above BTE equations in the metal film. The simulation domain is divided into discrete grids (finite volumes) of size Δx^d, with d denoting the dimension. In the two-temperature BTE, Eqs. 1(a) and 1(b) are discretized as follows:

$$e_{e,\alpha,x+\Delta x_e,t+\Delta t} = (1 - w_e)e_{e,\alpha,x,t} + w_e e^0_{e,\alpha,x,t} - G_{ep}\left[\frac{e^0_{e,\alpha,x,t}}{c_e} - \frac{e^0_{p,\alpha,x,t}}{c_p}\right]\Delta t, \tag{2a}$$

$$e_{p,\alpha,x+\Delta x_p,t+\Delta t} = (1 - w_p)e_{p,\alpha,x,t} + w_p e^0_{p,\alpha,x,t} + G_{ep}\left[\frac{e^0_{e,\alpha,x,t}}{c_e} - \frac{e^0_{p,\alpha,x,t}}{c_p}\right]\Delta t, \tag{2b}$$

where α is the index for transport directions, which is either forward + or backward – in the 1D BTE here. e_e^0 and e_p^0 are the equilibrium energy density of electrons and phonons, which are approximated as $(e_{e,+} + e_{e,-})/2$ and $(e_{p,+} + e_{p,-})/2$, respectively. In addition, $w_e = \Delta t/\tau_e$ and $w_p = \Delta t/\tau_p$, where τ_e and τ_p denote the relaxation time of electrons and phonons, respectively. In this work, the computational grid size is mode-dependent, that is, $\Delta x_e = v_e \Delta t$ and $\Delta x_p = v_p \Delta t$, which is different from the mode-dependent time step size scheme used in previous LBM-based BTE calculations.[27] We note that $v_e \gg v_p$ in most metals and semiconductors, with the former usually being close to the Fermi velocity v_f (on the order of 1×10^6 m/s) and the latter approximately being the phonon group velocity v_s (on the order of 1×10^3 m/s). The great mismatch between v_f and v_s makes Δx_e and Δx_p differ by almost three orders of magnitude. As a result, each electron grid is coupled to thousands of phonon grids.

The fact that the thickness of the thin film is usually between 20 and 200 nm while the substrate is usually much thicker renders a full BTE calculation for both sides rather computationally demanding, especially when multiple phonon modes or electron modes are included. Because the substrate is usually much thicker than the mean-free-path of the heat carriers, we use the diffusive TTM

$$C_e \frac{\partial T_e}{\partial t} = \nabla \cdot (\kappa_e \nabla T_e) - G_{ep}(T_e - T_p) + \dot{r}_e, \tag{3a}$$

$$C_p \frac{\partial T_p}{\partial t} = \nabla \cdot (\kappa_p \nabla T_p) + G_{ep}(T_e - T_p) + \dot{r}_p, \tag{3b}$$

to model the heat transfer in the substrate. In the above equations, C, T, κ, and $\dot{r}$ are the heat capacity, temperature, thermal conductivity, and volumetric heat generation rate of electrons (subscript e) and phonons (subscript p), respectively.

In the diffusive TTM calculation, the phonon channel and the electron channel are discretized uniformly with the same Δx_F, and Eqs. 3(a) and 3(b) are discretized and rearranged as

$$T_{e,x,t+\Delta t} = (1 - 2\alpha_e - \beta_{ep})T_{e,x,t} + \alpha_e(T_{e,x+\Delta x_F,t} + T_{e,x-\Delta x_F,t}) + \beta_{ep}T_{p,x,t}, \tag{4a}$$

$$T_{p,x,t+\Delta t} = (1 - 2\alpha_p - \beta_{pe})T_{p,x,t} + \alpha_p(T_{p,x+\Delta x_F,t} + T_{p,x-\Delta x_F,t}) + \beta_{pe}T_{e,x,t}, \tag{4b}$$

where $\alpha_e = \Delta t\kappa_e/[c_e(\Delta x_F)^2]$, $\beta_{ep} = \Delta t G_{ep}/c_e$, $\alpha_p = \Delta t\kappa_p/[c_p(\Delta x_F)^2]$, and $\beta_{pe} = \Delta t G_{ep}/c_p$. This coupled BTE-Fourier scheme is able to capture the ballistic nature of heat transfer in the metal film and account for the diffusive thermal transport inside the substrate effectively and efficiently, which has been used for phonon transport previously.[28]

III. INPUT PARAMETERS

The BTE simulation described in Section II requires several input parameters: velocity v, heat capacity c (or the electron heat capacity constant γ), and lifetime τ of electrons and phonons, as well as the electron-phonon coupling constant G_{ep}. The values of v_e, γ, and G_{ep} can be obtained from literature, while the calculation of other parameters is presented in this section.

A. Bulk properties: v_p, c_p, τ_p, and τ_e

In metals, both phonon and electron contribute to thermal transport. As the total thermal conductivity κ_{tot} and electrical conductivity σ of metals are usually available, one can roughly estimate the phononic part based on

$$\kappa_{tot} = \kappa_p + \kappa_e, \tag{5}$$

in which the electronic thermal conductivity κ_e can be estimated by the Wiedemann-Franz law

$$\kappa_e = LT\sigma, \tag{6}$$

where L is the Lorenz number. The Sommerfeld value of 2.44×10^{-8} WΩK^{-2} was derived for L in degenerate metals, semi-metals, or semiconductors. However, we note that Eq. (5) is a rather rough approach to estimate κ_p.[29] Herein we adopt the κ_p, heat capacity, and phonon dispersion relations obtained from first-principles calculations.[30] We will solve the BTE equations under a gray approximation where average phonon properties are used. v_p is calculated as the average Brillouin Zone center group velocity (in the Γ-X direction) of the three acoustic branches as

$$v_p^{-1} = (v_{LA}^{-1} + v_{TA,1}^{-1} + v_{TA,2}^{-1})/3, \tag{7}$$

where LA and TA (two branches) denote the longitudinal and transverse acoustic branch, respectively. The average phonon relaxation time τ_p is estimated from the kinetic theory

$$\kappa_p = c_p v_p^2 \tau_p/3. \tag{8}$$

It is worth mentioning that even though such gray approximation has been widely used to interpret experiments, it inherently neglects the influence of spectral phonon and electron properties on heat transfer. In this work, we deliberately choose to use a gray model because it is accurate enough to capture the effect of interlayer on the overall heat transfer characteristics of the system of interest, while a more complicated spectral model is not necessary.

After we obtain κ_p, κ_e can be obtained by Eq. (5) with a knowledge of the experimental value of the total thermal conductivity. The relaxation time of electrons can be estimated in a similar way as Eq. (8) for phonons. Table I lists the average phonon and electron properties of Au, Al, Pt, and Si to be used in the BTE simulations.

B. Interfacial thermal transport properties

1. Phonon transmission

When two materials with dissimilar vibrational properties like those in Fig. 1(a) are put into contact, phonons attempting to traverse the interface might be reflected, leading to interfacial thermal resistance R_{pp}, of which the inverse is often referred to as interfacial thermal conductance G_{pp}. R_{pp} can be estimated by approaches such as molecular dynamics simulations, acoustic mismatch model,[34] diffuse mismatch model[35] (DMM), and nonequilibrium Green's function approach.[36] DMM cannot capture the effect of coherent phonon transport on phonon transmission as observed in systems containing multiple smooth, parallel interfaces.[13,15,37] However, it was developed based on the assumption of diffuse phonon interface scattering, which at the same time also suppresses coherent phonon transport.[13,15] Therefore, we limit this work to systems with rough interfaces and use DMM to calculate phonon transmission coefficients. In this work, the R_{pp} between two materials is computed using full phonon dispersion relations over the entire first Brillouin zone (FBZ) as[38]

$$R_{pp}^{-1} = G_{pp} = \frac{1}{V_{\mathrm{FBZ}} N_k} \sum_{\nu\mathbf{k}, v_{\nu\mathbf{k}Ax}>0} \frac{(\hbar\omega_{\nu\mathbf{k}})^2}{k_B T^2} v_{\nu\mathbf{k}Ax} \Xi_{AB,\nu\mathbf{k}} \times f(\omega_{\nu\mathbf{k}}, T)[f(\omega_{\nu\mathbf{k}}, T) + 1], \tag{9}$$

where V_{FBZ} is the volume of the FBZ, $\hbar$ is the reduced Planck constant, and N_k is the number of grids we have divided the FBZ into, that is, $16 \times 16 \times 16$ uniform grids of volume ΔV_A and ΔV_B. In addition, $v_{\nu\mathbf{k}Ax}$ is the group velocity of a phonon mode with wavevector $\mathbf{k}$ and polarization ν in material A projected in the x direction, and f is the distribution function. The elastic phonon transmission coefficient Ξ_{AB} for phonon transmission from material A to material B is calculated using DMM as

$$\Xi_{AB}(\omega) = \frac{\Delta V_B \sum_{\nu\mathbf{k}} v_{\nu\mathbf{k}Bx} \delta_{\omega_{\nu\mathbf{k}},\omega}}{\Delta V_A \sum_{\nu\mathbf{k}} v_{\nu\mathbf{k}Ax} \delta_{\omega_{\nu\mathbf{k}},\omega} + \Delta V_B \sum_{\nu\mathbf{k}} v_{\nu\mathbf{k}Bx} \delta_{\omega_{\nu\mathbf{k}},\omega}}, \tag{10}$$

where $\delta_{\omega_{\nu\mathbf{k}},\omega}$ is the Kronecker delta function. The R_{pp}'s of Au-Si, Au-Al, Au-Pt, Al-Si, and Pt-Si as a function of temperature computed in this way are plotted in Fig. 1(b). It is worth mentioning that the vibrational density of states of Al and Pt are between those of Au and Si, as shown in Fig. 1(a). As a result, both the G_{pp} of Au-Al/Pt and that of Al/Pt-Si are higher than the G_{pp} of Au-Si. Therefore, adding a thin layer of Al or Pt to Au-Si interface should not increase the effective interfacial thermal resistance significantly in terms of phonon transport. Later we will see that a thin Al or Pt interlayer could even enhance interfacial thermal transport by reducing the nonequilibrium between electrons and phonons near the interface.

TABLE I. Average phonon and electron properties of Au, Al, Pt, and Si used in the BTE or Fourier calculations.

Quantity	Au	Al	Pt	Si
v_p ($\times 10^3$ m/s)	1.85	3.43	1.91	6.40
c_p ($\times 10^6$ J/m^3 K)	2.40	2.43	2.67	1.66
τ_p (ps)	0.95	0.58	1.79	6.53
κ_p (W/m K)	2.6	5.5	5.8	148.0
κ_{tot} (W/m K)	314.0[31]	205.0[31]	71.6[31]	148.0
κ_e (W/m K)	311.4	199.5	65.8	N/A
v_e ($\times 10^6$ m/s)	1.40[32]	2.03[32]	0.46	N/A
γ_e (W/m^3 K^2)	62.9[33]	91.2[33]	748.1[33]	N/A
τ_e (fs)	25.3	5.3	4.1	N/A
G_{ep} ($\times 10^{16}$ W/m^3 K)	2.6[33]	24.6[33]	108.7[33]	N/A

2. Electron transmission

Electron transmission across the interface between metal and low-doped semiconductor is usually a thermionic emission process, which has an effective thermal conductance lower than or comparable to its phonon counterpart.[18] Moreover, the very low density of free electrons (or holes) in the low-doped semiconductor renders it difficult for electronic heat to be dissipated further into the substrate.[18] Therefore, the electron transmission channel is negligible in metal-low-doped semiconductor systems.

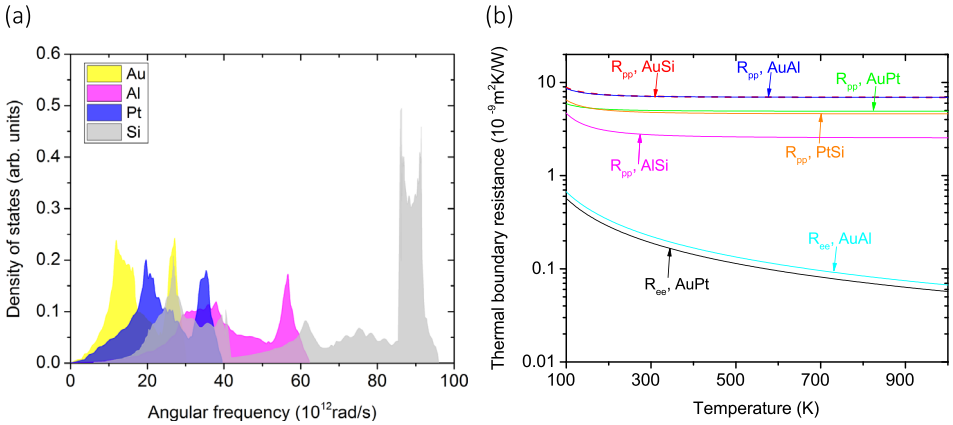

FIG. 1. (a) The vibrational density of states of Au, Al, Pt, and Si. (b) The interfacial thermal resistance, electronic (R_{ee}) or phononic (R_{pp}), for various interfaces.

For electron transport across the interface between two metals, Gundrum *et al.* extended the DMM for phonon to electron.[39] Specifically, the electronic interfacial thermal resistance R_{ee} can be computed as

$$R_{ee}^{-1} = G_{ee} = \frac{Z_A Z_B}{4(Z_A + Z_B)}, \tag{11}$$

where $Z_A = c_{e,A} v_{e,A}$ and $Z_B = c_{e,B} v_{e,B}$. As shown in Fig. 1(b), the computed R_{ee}'s are 1–2 orders of magnitude lower than corresponding R_{pp}'s but are very close to the R_{ee}'s measured in the experiments of Gundrum *et al.* for metal-metal interfaces.[39]

IV. SIMULATION RESULTS

A. Steady state thermal transport

In practical applications, a thin Cr, Ti, or Pt layer is usually deposited on the Si substrate before the deposition of the Au layer as an adhesion layer or diffusion barrier. It has been reported that a Ti interlayer at the Au-Si interface can enhance the effective thermal conductance significantly owing to the enhanced bonding at the interface.[11] We note that Al and Pt have 1–2 orders of magnitude higher G_{ep} than Au, which may reduce the interfacial thermal resistance due to electron-phonon nonequilibrium near the interface. To assess this effect, we calculate the effective R for Au-Si interfaces with and without an interlayer of Al or Pt, of which the schematics are shown in Fig. 2(a).

In our simulations, we maintain the surface of the Au film, as shown in Fig. 2(a), at 310 K while the bottom of the Si substrate at 290 K. The effective interfacial thermal resistance R_{eff} is computed as

$$R_{\text{eff}} = \frac{20\text{K}}{J} - \frac{l_{\text{Au}}}{\kappa_{\text{Au}}} - \frac{l_{\text{Si}}}{\kappa_{\text{Si}}}, \tag{12}$$

where J is the heat flux (in W/m^2), and l_{Au} and l_{Si} are the thickness of the Au and Si segment, respectively.

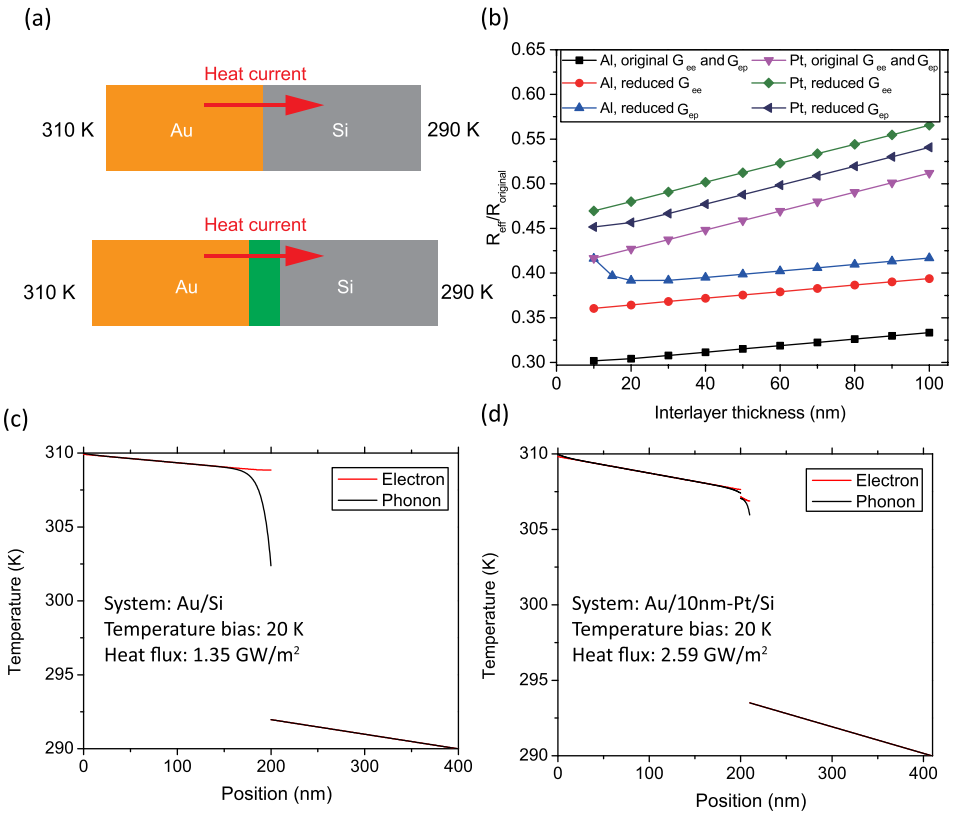

FIG. 2. (a) Schematic illustration of the simulated Au-Si and Au-interlayer-Si systems. (b) The ratio of the effective interfacial thermal resistance, R_{eff}, to the original interfacial thermal resistance, R_{original}, as a function of interlayer thickness. (c) and (d) Temperature profiles of electron and phonon obtained in the simulation.

In Fig. 2(b), we show the effective interfacial thermal resistance normalized by that of a direct Au-Si interface ($R_{original} = 1.33 \times 10^{-8}$ m^{2}K/W) as a function of interlayer thickness. To account for the possibility of non-ideal contact between the Au film and the interlayer, which causes lower G_{ee}, additional simulations using 20% of the theoretical value of G_{ee} predicted by Eq. (11) are also conducted. The artificially reduced G_{ee}'s are much lower than the experimental values for metal-metal interfaces reported in Ref. 39; therefore, we assert that it can well represent the lower limit of the G_{ee} of well-welded Au-Al and Au-Pt interfaces. As we can see in Fig. 2(b), for both ideal or non-ideal contact cases, the interfacial thermal resistance is reduced significantly by the interlayer, suggesting the robustness of this scheme to enhance interfacial thermal transport. R_{eff} is higher when G_{ee} is lower as it becomes more difficult for hot electrons in the Au film to transport into the Al or Pt interlayer and then equilibrate with phonons. Moreover, the effective interfacial thermal resistance R_{eff} increases with interlayer thickness, since the thermal resistance of the interlayer itself increases as $l_{interlayer}/\kappa_{interlayer}$.

Figures 2(c) and 2(d) are the temperature profiles of electron and phonon obtained in our simulations on Au-Si and Au-Pt-Si systems. A notable electron-phonon nonequilibrium region can be seen near the interface in Fig. 2(c), while this region is significantly reduced by the Pt interlayer, as shown in Fig. 2(d). The elimination of the nonequilibrium region leads to reduced R_{eff}, as suggested theoretically in Ref. 18.

Therefore, we conclude that interlayers can significantly affect the thermal transport across metal/dielectric interfaces if the heat dissipation across the original interface is limited by large electron-phonon nonequilibrium. This is usually true for metals with weak electron-phonon coupling, for example, Cu, Ag, and Au, and interlayers with strong electron-phonon coupling, for example, Al, Pt, Cr, and Ti.

B. Ultrafast electron cooling in Au thin films

The pump-probe technique has been used to evaluate the electron-phonon coupling constant G_{ep} of metals. In a pump-probe measurement, a pump laser is injected to the metal thin film in which the temperature of electrons can be elevated to thousands of Kelvins in tens to hundreds of femtoseconds. Subsequently, the hot electrons are cooled down by the colder lattice, and the cooling curve allows one to evaluate G_{ep}. Similar process also happens in practical applications such as heat-assisted magnetic recording. In this section, we assess the effect of interlayers on hot electron cooling dynamics in Au thin films.

The simulations are conducted to mimic pump-probe experiments of Guo *et al.*,[40] in which a pump laser with a pulse width of 390 fs was used. All the parameters of the laser in our simulations are the same as those in Ref. 40. In Figs. 3(a) and 3(b), we show the possible heat transfer pathways in the Au-Si system without (a) and with (b) an interlayer. When Au is in direct contact with Si, initially hot electrons dissipate heat into the lattice through electron-phonon coupling, and then the hot Au lattice transfers heat into the Si lattice. When there is an interlayer between Au and Si, an additional channel is created, in which hot electrons carry heat into the interlayer and deposit heat into the interlayer lattice. If the interlayer has much higher G_{ep} than Au, the lattice temperature of the interlayer increases more quickly than Au. This leads to backflow of phononic heat from the interlayer to the Au lattice. The above heat transfer pathways are indicated as (I), (II), and (III), and their effect on lattice heating will be discussed later. The direction indicated by the dashed arrow for channel (III) is when the interlayer has lower G_{ep} than Au. In fact, another possible channel, direct coupling between electrons in the Au film and the substrate, may contribute to interfacial thermal conductance.[40–42] However, the existence of such electron-substrate coupling channel is neither unambiguously confirmed nor well understood.[42–45] Therefore, it is not considered at the moment in this paper.

As shown in Fig. 3(c), the electron temperature increases to 2000–3000 K within hundreds of femtoseconds and then decreases at a much lower speed. Moreover, adding an interlayer accelerates hot electron cooling substantially. The acceleration arises from the new electron cooling

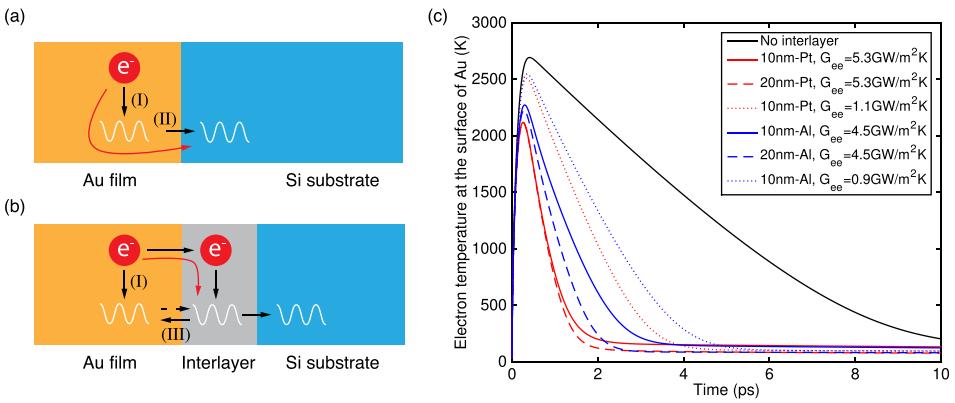

FIG. 3. (a) Heat transfer channels in Au-Si without an interlayer. (I) and (II) denote lattice heat transfer channels, with (I) denoting electron-phonon coupling while (II) denoting phonon transmission into the substrate. (b) Heat transfer channels in Au-Si with an interlayer. (I) denotes the same process as that in (a), while (III) denotes backflow of heat from the hotter interlayer lattice to the Au lattice. The heat flow direction indicated by the dashed arrow is also possible, for example, when G_{ep} of the interlayer is lower than that of Au. (c) Transient electron temperature at the surface of an Au thin film for different interlayer thickness, G_{ee} between Au film and interlayer, and interlayer material.

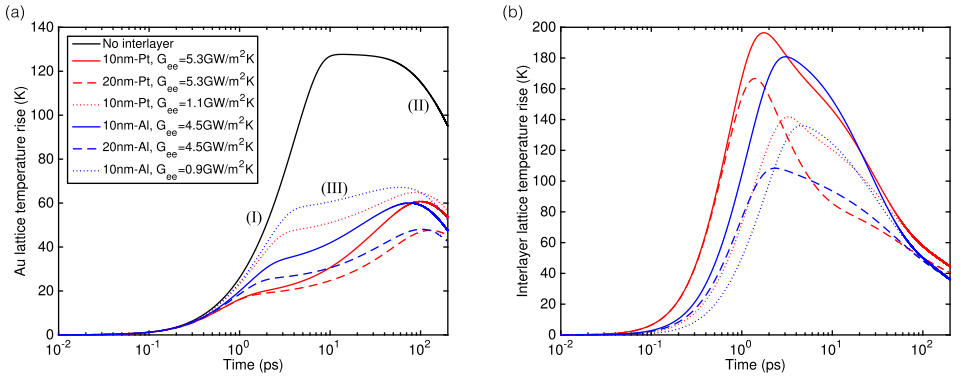

FIG. 4. (a) Lattice temperature rise of the Au film as a function of time for different interlayer thickness or G_{ee}. A laser fluence of 20 J/m^2 is used for all cases. The heating or cooling of the Au lattice is dominated by different mechanisms at different stages: (I) heat transfer from hot electrons, (II) heat dissipation into the substrate, and (III) backflow of heat from the hotter interlayer lattice. (b) Lattice temperature rise of the interlayer as a function of time.

channel created by the interlayer, as shown in Fig. 3(b). Specifically, hot electrons in Au can readily transmit across the Au-Al or Au-Pt interface and then rapidly dissipate heat into the Al or Pt lattice due to their high G_{ep}. To consider the effect of interface nonideality, we also conduct additional simulations in which we reduce the G_{ee} of Au-interlayer interface to 20% of the theoretical value. It is obvious that even for the reduced G_{ee} cases, a Pt or Al interlayer can accelerate hot electron cooling substantially. We also study the effect of interlayer thickness by simulating two different structures: one with a 10-nm thick interlayer while the other with a 20-nm interlayer. As shown in Fig. 3(c), electron temperature drops more quickly in the case with thicker interlayer. This is because a thicker interlayer has a larger volume V to absorb electronic heat through electron-phonon coupling, of which the heat transfer rate is on the order of $G_{ep,\text{interlayer}}V_{\text{interlayer}}$.

In Fig. 4(a), we show the lattice temperature rise ($T_p - 300$ K) as a function of time. As we can see, the lattice temperature of the Au film in the no-interlayer case increases at the beginning due to electron-phonon coupling (channel I), and decreases thereafter due to heat dissipation into the substrate (channel II). The above two competing processes, I and II, lead to a maximum lattice temperature ($T_{p,max}$), which is an important factor determining the lifetime of devices. In many applications, a high $T_{p,max}$ degrades or even destroys the device and therefore should be minimized. As we can see, adding an interlayer of Al or Pt helps to reduce $T_{p,max}$ significantly. For the cases with interlayers, as shown in Fig. 4(a), the lattice temperature of Au increases at two distinctly different speeds. Similar to the no-interlayer case, the initial fast increase in T_p is due to electron-phonon coupling, while the subsequent slower increase is caused by phononic heat transfer from the hotter lattice of the interlayer (channel III). Moreover, thicker interlayer or higher G_{ee} between the Au film and the interlayer reduces $T_{p,max}$ more significantly.

The above observations can be understood more clearly by Fig. 4(b), where we plot the lattice temperature rise in the interlayer as a function of time. Comparing Figs. 4(a) and 4(b), we can see that the temperature rise in the interlayer is much higher than that in the Au film. This is because the hot electrons in the Au film transfer heat into the interlayer quickly due to the high G_{ee} and then dissipate heat into the interlayer lattice rapidly due to the high G_{ep}. The above channel is much more efficient in transferring heat from hot electrons to the lattice than the electron-phonon coupling channel in the Au film, which has much lower G_{ep} than Pt and Al. As a result, most of the electron energy is deposited into the interlayer lattice rather than the Au lattice. Similar sub-surface heating phenomena have been observed for Au-Cr multilayers,[17] Ag film-Cu substrate systems,[46,47] and Au-Pt bilayers.[48] Moreover, a higher G_{ee} leads to faster transfer of electronic heat from Au film to the interlayer and a thicker interlayer has a larger volume to absorb electronic heat, of which both reduce the lattice temperature rise in Au.

As a final remark of this section, we note that adding an interlayer of Al or Pt to the Au-Si interface has two-fold effects on the heat transfer characteristics of the system. On one hand, it accelerates hot electron cooling and thereby causes more energy loss, which should be minimized for energy efficiency; on the other hand, it reduces lattice heating in the Au thin film significantly, which could assist in maintaining a longer device lifetime. This means that sophisticated thermal design is needed to achieve an optimal balance between device performance and lifetime.

V. CONCLUSION

In this work, we conducted BTE simulations to study electron-phonon coupled thermal transport in Au-Si systems. We demonstrated that by applying an interlayer with stronger electron-phonon coupling than the original metal film, the effective interfacial thermal resistance can be significantly reduced. This is because the interlayer can drag electrons and phonons back into equilibrium efficiently, thereby reducing the resistance caused by the nonequilibrium between electrons and phonons. Moreover, we observed that interlayers can also cause a faster energy loss of hot electrons. The reduced interfacial resistance and accelerated electron cooling impose a tradeoff between the lifetime and the energy efficiency of the device, which requires sophisticated thermal design.

ACKNOWLEDGMENTS

The authors thank the support from the Airforce Office of Scientific Research (AFOSR). Yan Wang would like to thank Dr. Liang Guo for fruitful discussions on pump-probe experiments.

[1]P. E. Phelan, J. Heat Transfer **120**, 37 (1998).
[2]F. Kargar, S. Ramirez, B. Debnath, H. Malekpour, R. K. Lake, and A. A. Balandin, Appl. Phys. Lett. **107**, 171904 (2015).

[3]J. D. Renteria, S. Ramirez, H. Malekpour, B. Alonso, A. Centeno, A. Zurutuza, A. I. Cocemasov, D. L. Nika, and A. A. Balandin, Adv. Funct. Mater. **25**, 4664 (2015).
[4]M. Shtein, R. Nadiv, M. Buzaglo, and O. Regev, ACS Appl. Mater. Interfaces **7**, 23725 (2015).
[5]J. Renteria, S. Legedza, R. Salgado, M. Balandin, S. Ramirez, M. Saadah, F. Kargar, and A. Balandin, Mater. Des. **88**, 214 (2015).
[6]Y. Wang, S. Chen, and X. Ruan, Appl. Phys. Lett. **100**, 163101 (2012).
[7]Y. Wang, A. Vallabhaneni, J. Hu, B. Qiu, Y. P. Chen, and X. Ruan, Nano Lett. **14**, 592 (2014).
[8]Y. Wang, A. K. Vallabhaneni, B. Qiu, and X. Ruan, Nanoscale Microscale Thermophys. Eng. **18**, 155 (2014).
[9]P. E. Hopkins, L. M. Phinney, J. R. Serrano, and T. E. Beechem, Phys. Rev. B **82**, 85307 (2010).
[10]M. D. Losego, M. E. Grady, N. R. Sottos, D. G. Cahill, and P. V. Braun, Nat. Mater. **11**, 502 (2012).
[11]B. F. Donovan, C. J. Szwejkowski, J. C. Duda, R. Cheaito, J. T. Gaskins, C.-Y. Peter Yang, C. Constantin, R. E. Jones, and P. E. Hopkins, Appl. Phys. Lett. **105**, 203502 (2014).
[12]R. Gulotty, M. Castellino, P. Jagdale, A. Tagliaferro, and A. A. Balandin, ACS Nano **7**, 5114 (2013).
[13]Y. Wang, H. Huang, and X. Ruan, Phys. Rev. B **90**, 165406 (2014).
[14]X. Mu, T. Zhang, D. B. Go, and T. Luo, Carbon **83**, 208 (2015).
[15]Y. Wang, C. Gu, and X. Ruan, Appl. Phys. Lett. **106**, 073104 (2015).
[16]T. English, J. Duda, J. Smoyer, D. Jordan, P. Norris, and L. Zhigilei, Phys. Rev. B **85**, 035438 (2012).
[17]T. Qiu and C. Tien, Int. J. Heat Mass Transfer **37**, 2789 (1994).
[18]Y. Wang and X. Ruan, in *ASME 2013 Heat Transfer Summer Conference Collocated with the ASME 2013 7th International Conference on Energy Sustainability and the ASME 2013 11th International Conference on Fuel Cell Science, Engineering and Technology* (American Society of Mechanical Engineers, 2013), p. V001T03A041.
[19]A. Giri, J. T. Gaskins, B. F. Donovan, C. Szwejkowski, R. J. Warzoha, M. A. Rodriguez, J. Ihlefeld, and P. E. Hopkins, J. Appl. Phys. **117**, 105105 (2015).
[20]A. Majumdar and P. Reddy, Appl. Phys. Lett. **84**, 4768 (2004).
[21]Y. Wang, X. Ruan, and A. K. Roy, Phys. Rev. B **85**, 205311 (2012).
[22]P. M. Norris, A. P. Caffrey, R. J. Stevens, J. M. Klopf, J. James, T. McLeskey, and A. N. Smith, Rev. Sci. Instrum. **74**, 400 (2003).
[23]R. Escobar, B. Smith, and C. Amon, J. Electron. Packag. **128**, 115 (2006).
[24]F. N. Donmezer, D. Singh, W. James, A. Christensen, S. Graham, and J. Y. Murthy, ASME Conf. Proc. **2011**, 333.
[25]In the Sommerfeld free electron model, $C_e = \gamma_e T_e$. Therefore, $e_e = \int_0^{T_e} C_e dT = 0.5\gamma_e T_e^2$.
[26]S. S. Ghai, W. T. Kim, R. A. Escobar, C. H. Amon, and M. S. Jhon, J. Appl. Phys. **97**, 10P703 (2005).
[27]D. Sellan, J. Turney, A. McGaughey, and C. Amon, J. Appl. Phys. **108**, 113524 (2010).
[28]J. M. Loy, D. Singh, and J. Y. Murthy, in *ASME 2009 Heat Transfer Summer Conference Collocated with the InterPACK09 and 3rd Energy Sustainability Conferences* (American Society of Mechanical Engineers, 2009), pp. 601–610.
[29]For example, the κ_p of Nickel based on Eq. (5) is $91\,\mathrm{W/m\,K} - 2.44 \times 10^{-8} \times 300 \times 1.43 \times 10^{7}\,\mathrm{W/m\,K} = -14\,\mathrm{W/m\,K}$, which is not physical.
[30]Y. Wang, Z. Lu, and X. Ruan, "First principles calculation of lattice thermal conductivity of metals considering phonon-phonon and phonon-electron scattering" (unpublished).
[31]F. W. Sears, M. W. Zemansky, and H. D. Young, *University Physics* (Addison-Wesley, 1982).
[32]N. Ashcroft, *Solid State Physics* (Saunders College, Philadelphia, 1976).
[33]Z. Lin, L. V. Zhigilei, and V. Celli, Phys. Rev. B **77**, 075133 (2008).
[34]I. Khalatnikov, Zh. Eksp. Teor. Fiz. **22**, 687 (1952).
[35]E. T. Swartz and R. O. Pohl, Rev. Mod. Phys. **61**, 605 (1989).
[36]W. Zhang, T. Fisher, and N. Mingo, Numer. Heat Transfer, Part B **51**, 333 (2007).
[37]J. Shi, Y. Dong, T. Fisher, and X. Ruan, J. Appl. Phys. **118**, 044302 (2015).
[38]P. Reddy, K. Castelino, and A. Majumdar, Appl. Phys. Lett. **87**, 211908 (2005).
[39]B. C. Gundrum, D. G. Cahill, and R. S. Averback, Phys. Rev. B **72**, 245426 (2005).
[40]L. Guo, S. L. Hodson, T. S. Fisher, and X. Xu, J. Heat Transfer **134**, 042402 (2012).
[41]P. E. Hopkins and P. M. Norris, in *Proceedings of the Fifth International Conference on Photo-Excited Processes and Applications (5-ICPEPA)* [Appl. Surf. Sci. **253**, 6289 (2007)].
[42]A. Giri, B. M. Foley, and P. E. Hopkins, J. Heat Transfer **136**, 092401 (2014).
[43]P. E. Hopkins, J. C. Duda, B. Kaehr, X. W. Zhou, C.-Y. P. Yang, and R. E. Jones, Appl. Phys. Lett. **103**, 211910 (2013).
[44]L. Guo and X. Xu, J. Heat Transfer **136**, 122401 (2014).
[45]Z. Lu, Y. Wang, and X. Ruan, "Metal/dielectric thermal interfacial transport considering cross-interface electron-phonon coupling: Theory, two-temperature molecular dynamics, and thermal circuit," Phys. Rev. B (to be published)
[46]D. A. Thomas, Z. Lin, L. V. Zhigilei, E. L. Gurevich, S. Kittel, and R. Hergenröder, Appl. Surf. Sci. **255**, 9605 (2009).
[47]C. Wu, D. A. Thomas, Z. Lin, and L. V. Zhigilei, Appl. Phys. A **104**, 781 (2011).
[48]G.-M. Choi, R. Wilson, and D. G. Cahill, Phys. Rev. B **89**, 064307 (2014).
[49]Y. Wang, B. Qiu, and X. Ruan, Appl. Phys. Lett. **101**(1), 013101 (2012).